P- ISSN 1991-8941 E-ISSN 2706-6703
2021,15 (2) :74 –82

Journal of University of Anbar for Pure Science (JUAPS)

Open Access

Synthesis and Characterization of Spinel Ferrite $Co_{0.8}Fe_{2.2}O_4$ Nanoparticle

Mohammed B. Jumaa,[a*] Tahseen H Mubarak[a], Ali. M. Mohammad[b]
[a]University of Diyala, College of Science, Department of Physics, Diyala, Iraq.
[b]University of Garmian, College of Education, Department of Physics, Garmian, Iraq.

ARTICLE INFO

Received: 9 / 7 /2020
Accepted: 7 /8 / 2021
Available online: 21 / 12 / 2021

DOI:
http://dx.doi.org/10.37652/JUAP
2021.15.2.11

Keywords:
Nanoparticle ferrites;
Spinel ferrites;
X-ray diffraction;
FE-SEM;
Dielectric properties.

ABSTRACT

Cobalt ferrite $Co_{0.8}Fe_{2.2}O_4$ nanoparticles were prepared using the sol-gel auto combustion process. The effects of calcination temperature on structural, magnetic, and electrical properties were studied. The cubic spinel phase fashioning of ferrite structure was confirmed using Fourier Transform-Infrared Spectroscopy (FT-IR) and X-ray Diffraction Patterns (XRD). The size of the formed crystallite of ferrite samples is ranged from 24.530 to 49.067 nm and it is found to be dependent on calcination. According to the images, which were taken by a Field Emission-Scanning Electron Microscope (FE-SEM), the particle size increases with raising the calcination temperature. Energy Dispersive Spectrum (EDS) was used to confirm the presence of Co, Fe, and O in all samples. A Vibrating Sample Magnetometer (VSM) was used to study the magnetic properties such as coercivity, saturation magnetization, and remanence field for the as-burnt and calcined samples. All samples exhibited ferrimagnetic behavior. As the calcination temperature rises, saturation magnetization (M_s), remanent magnetization (M_r), and squareness ratio (M_r/M_s) increased. This behavior is related to the spin canting and disturbance in the surface spin. At room temperature, the dielectric loss factor (ε''), dielectric loss angle ($tan\delta$), dielectric constant (ε'), and the conductivity σ_{ac} of all samples were examined as a function of frequency using the LCR meter. The changes in dielectric properties have been characterized at frequencies ranged from 50Hz to 2MHz based on Koop's theory, Maxwell-Wagner polarization, and electron hopping. As frequency rose, all-dielectric properties exhibited natural behavior.

1. INTRODUCTION

Metal oxide in the nano-regime has piqued the interest of many researchers in recent years because of its potential use in magnetic recording, biomedicine, spintronics, ferro-fluids, magnetic drug targeting, gas sensors, and hyperthermia for cancer treatment [1-3]. Spinel cobalt ferrite is a promising material for many commercial applications because of its mechanical hardness, moderate saturation magnetization, high coercivity, and excellent chemical stability [4,5]. Nano-ferrites are excellent magnetic and dielectric materials. The ferrites' characteristics are determined by the metal cations used and their distribution between the spinel lattice's tetrahedral (A) and octahedral (B) sites. The preparation circumstances, sintering temperature, chemical composition, and preparation technique all influence the characteristics of nano-ferrites [6].

*Corresponding author: Department of Physics, College of Education for Pure Sciences University Of Diyala, Iraq. Tel.: +964 7719910896 ORCID:0000-0003-1778-6137 . E-mail address: sciphyms06@uodiyala.edu.iq

For the production of stoichiometric ferrites nanoparticles, several chemical and physical processes such as sol-gel, hydrothermal, co-precipitation, combustion technique, ball-milling, and so on have been applied [7].

The structural, magnetical, and electrical properties of cobalt ferrite are affected by a variety of characteristics in the spinel cobalt ferrite structure, including crystallite size, particle size, metal cation distribution among the lattice sites, and porosity [8]. The magnetic properties, such as saturation magnetization (M_S), remnant magnetization (M_r), and coercivity (H_C) cobalt ferrite, are strongly affected by the increase of calcination temperature [9,10]. Furthermore, the dielectric properties of cobalt ferrite are highly impacted by cation redistributions as the calcination temperature rises, making them appealing for high-frequency applications [10]. In this study, $Co_{0.8}Fe_{2.2}O4$ nanoparticles were synthesized using a sol-gel auto combustion method because it is simple to make, has high purity, requires little time, and has good uniformity at low temperatures [11].

2. EXPERIMENTAL DETAILS

2.1. Synthesis

The sol-gel auto combustion method was used to create nano-crystalline cobalt ferrites having the empirical formula $Co_{0.8}Fe_{2.2}O_4$. To form a mixed solution, the stoichiometric concentrations of citric acid $C_6H_8O_7.H_2O$, ferric nitrate $Fe(NO_3)_3.9H_2O$, and cobalt nitrate $Co(NO_3)_2.6H_2O$ in a 1:1 mole ratio were dissolved separately in minimal quantities of deionized water. The resulting solutions were converted into a viscous gel-phase by gradually raising the hot plate temperature to 90 °C for 2 hours under continuous stirring. During evaporation, the solution became viscid and subsequently transformed into a viscid brown gel. After separating the water molecules, which were in the mixture, the viscid gel was placed in an oven and heated to 250 °C to initiate an auto combustion reaction and create as-burnt ferrite powder. The rough powder was collected and processed in a mortar with an agitating unite to produce a soft powder. The as-burnt powder after combustion was calcined at 500, 600, and 700 ˚C for 3 hours to increase the homogeneity and to remove the organic waste, where the as-burnt samples and the samples that calcined at 500, 600, and 700 ˚C added with a four-drop PVA as a binder to press it into circular pellets of diameter 13 mm with thickness about 2 mm. This occurs by applying a pressure of 2 tons for 1 min using a hydraulic press by dry pressing method, then the prepared pellets were sintered at 350, 600, 700, and 800 ℃ for 3hours to intensify the samples and, slowly allowed to be cooled naturally to examine the dielectric properties.

2.2. Characterizations

XRD patterns were recorded using a (PANalytical X'pert Pro diffractometer, Netherlands) equipped with a source of high-intensity Cu kα radiation (λ= 0.154 nm, 40 mA, 40 kV) in the 2θ range (15° - 70°). The surface morphology of the samples was carried out by FE-SEM using (FE-SEM; Model Mira3-XMU, TESCAN, Japan). Fourier transform-infrared studies were carried for all the samples using (Perkin Elmer FT-IR spectrometer, USA) and KBr pellets in the range 300 to 4000 cm^{-1}.

The results for remanence, magnetization, and coercive fields were obtained by tracing M–H hysteresis loops of calcined powders for as-burnt, 500, 600, and 700 C using an (LBKFB model Meghnatis Daghigh Kavir Company) by Vibrating Sample Magnetometer (VSM) at room temperature in applied fields ± 15kOe. At room temperature, dielectric measurements were taken with an LCR meter type (KEYSIGHT E4980A) in the frequency range 50Hz to 2MHz.

3. RESULTS AND DISCUSSION

3.1. Structural Properties

Figure 1 represents the XRD patterns of $Co_{0.8}Fe_{2.2}O_4$ nanoferrites as-burnt and calcined powders at temperatures of 500, 600, and 700 degrees Celsius. All of the reflection peaks corresponding to the (111), (220), (311), (222), (400), (422), (511), and (440) planes of a cubic unit cell are visible in the XRD pattern. The peak location in XRD patterns matches the crystalline phase for $CoFe_2O_4$ with reference code ICSD 00-001-1121. Our findings show that the diffraction peaks become sharper and narrower as the calcination temperature rises, and their intensity rises as well. This signifies that crystallinity is intensifying when the crystalline volume ratio increases due to the nuclei's particle size enlargement [12]. The results agreed well with what was reported by Ali et al. [13]. The impure phase of hematite (iron oxide) was found in samples calcined at 600 and 700 ℃ [12]. The crystallite sizes (D) were estimated from Scherrer formula [14] for each sample using the peak's FWHM (311).

$$D = \frac{0.96\lambda}{\beta.cos\theta} \qquad (1)$$

Where D is the crystalline size, λ the wavelength of X-ray, β (in radians) is FWHM of the concerned peak, and θ is the Bragg diffraction angle. Table 1 shows with the raise of crystalline size the calcination temperature. It is noticed that the particle's specific surface area is reduced, which is agreed with reported in earlier research [15].

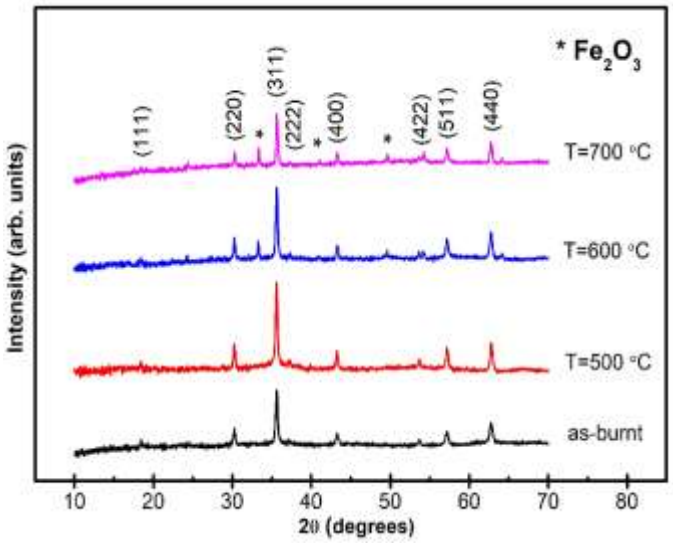

Fig1: The XRD pattern of $Co_{0.8}Fe_{2.2}O_4$ nanoferrites for as-burnt and different calcination temperatures (500, 600, and 700 °C).

The lattice parameter (a) of $Co_{0.8}Fe_{2.2}O_4$ nanoferrites was determined by interplanar spacing using the following relationship [16].

$$a = d_{hkl}\sqrt{h^2 + k^2 + l^2} \qquad (2)$$

Where h, k and l are the Miller indices of the lattice plane and d_{hkl} is interplanar spacing. As shown in table 1, the measured lattice parameters revealed that the lattice parameter is 8.360 Å, 8.368 Å, 8.353 Å, and 8.348 Å for all samples (as-

burnt, 500 ℃, 600 ℃, and 700 ℃), respectively. Except for calcination at 500 ℃, the lattice parameter appears to decrease as the calcination temperature rises. These behaviors agree with those found in the literature [17].

The prepared samples' X-ray density (ρ_x) was determined using the equation [13].

$$\rho_x = \frac{8M}{Na^3} \qquad (3)$$

where factor 8 indicates the number of molecules per unit cell, N is Avogadro's number, M is the molecular weight and a^3 is the cell volume. The X-ray densities of cobalt ferrite samples ranged between 5.315 g/cm^3 and 5.354 g/cm^3. The X-ray densities increased as the calcination temperature increased. This is consistent with the preceding article [18].

The distance between hopping lengths in the tetrahedral (A) and octahedral (B) sites for $Co_{0.8}Fe_{2.2}O_4$ nanoferrites and the magnetic ions were calculated by utilizing the relations below [19].

$$L_A = 0.25a\sqrt{3} \qquad (4)$$

$$L_B = 0.25a\sqrt{2} \qquad (5)$$

The measured hopping length L_A and L_B values for $Co_{0.8}Fe_{2.2}O_4$ nanoparticles are presented in table 1. It is noted that as calcination temperature increases, the hopping length changes. The rate at which Fe^{3+} substitutes into the tetrahedral and octahedral sites changes as Fe^{3+} concentration increases, which may play a role in changing the value of hopping length concerning the fluctuation in the ionic radius of Co^{2+} and Fe^{3+} ions.

Table 1. Crystallite size (D), Lattice parameter 'a', X-ray density (ρ_x), hopping length (L_A)and (L_B) of $Co_{0.8}Fe_{2.2}O_4$ nanoferrites for as-burnt and different calcination temperature (500, 600, and 700 °C).

Composition	Temp.℃	D(nm)	A (Å)	ρ_x (g/cm^3)	L_A (Å)	L_B (Å)
($Co_{0.8}Fe_{2.2}O_4$)	as- burnt	24.53	8.36	5.330	3.620	2.955
	500	27.90	8.36	5.315	3.623	2.958
	600	36.26	8.35	5.344	3.617	2.9532
	700	49.06	8.34	5.354	3.614	2.951

3.2. Fourier Transform Infrared Spectroscopy (FT-IR):

Based on vibrational modes, the FT-IR spectrum analysis is a valuable technique for determining where ions are situated in the crystal structure [20]. Fig.2 shows the FT-IR spectra of all the synthesized samples (as-burnt, 500, 600, and 700 ℃) respectively. It is noted that all spinel compounds conform to the vibrational modes of the two major absorption bands below 1000 cm^{-1}. The presence of the band in the 569.001 to 570.930 cm^{-1} (high frequency v_1) range coincides to the complexes of the tetrahedral (A-site) group vibration (M-O) whereas that in the range of 362.617 to 368.404 cm^{-1} (low frequency v_2) arises due to the octahedral (B-site) group complexes intrinsic vibrations (M-O). Table 2 shows the positions of bands v_1 and v_2 as a function of calcination temperature. The interaction of oxygen ions with cations in the unit cell's octahedral and tetrahedral sites could explain the frequency difference between the characteristic vibrations v_1 and v_2 [16]. The FT-IR analysis shows a rise in calcined temperatures (as-burnt, 500, and 600 °C), a similar pattern of peak shifting towards the higher frequencies side for the bands v_1 and a similar pattern of peak shifting towards the lower frequencies side for the bands v_2, which indicates a mixed spinel state of $Co_{0.8}Fe_{2.2}O_4$. This can be attributed to the change in the lengths of the bonds between metal ions and oxygen ions found at the tetrahedral and octahedral positions [16].

2.2. Specimens Preparation

The method (Hand lay-up molding) is used in preparing the samples because it is one of the easy, successful and common methods. Unsaturated polyester resin is prepared by adding a hardener to ratio (2g hardenes:100 g UPE) and well mix it by the electric mixer for a homogeneous mixture. Glass fiber and rock wool fibers were cut in (20 cm x 20 cm) dimensions, and added to unsaturated polyester with a volumetric fraction of (20%). The molding process carried out.

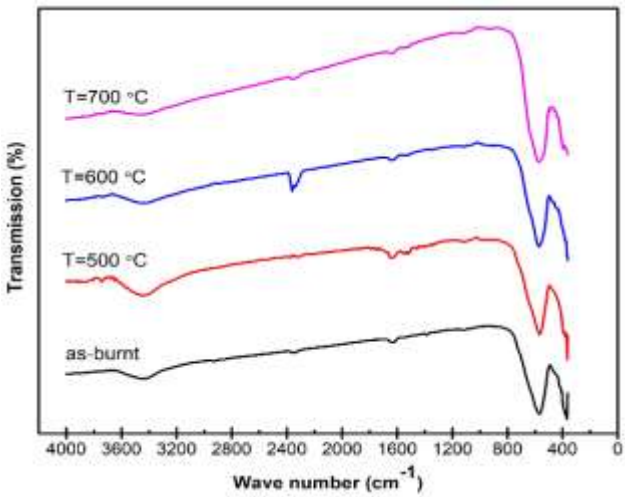

Fig 2: FT-IR spectra of $Co_{0.8}Fe_{2.2}O_4$ nanoferrites for as-burnt and different calcination temperatures (500, 600, and 700°C).

Table 2. Wave-number of FT-IR spectroscopy of $Co_{0.8}Fe_{2.2}O_4$ nanoferrites for as- burnt and different calcination temperatures (500, 600, and 700 °C).

Temp.℃	FT-IR frequency bands (cm^{-1})	
	v_1	v_2
as-burnt	569.001	368.404
500	569.001	366.475
600	570.930	362.617
700	570.930	362.617

3.3. FE-SEM Studies:

The particle size and surface morphology of as-burnt $Co_{1.2}Fe_{1.8}O_4$ nanoferrites and the calcined samples at different calcination temperatures were examined by the image of FE-SEM, as depicted in Fig. 3 (a–d).

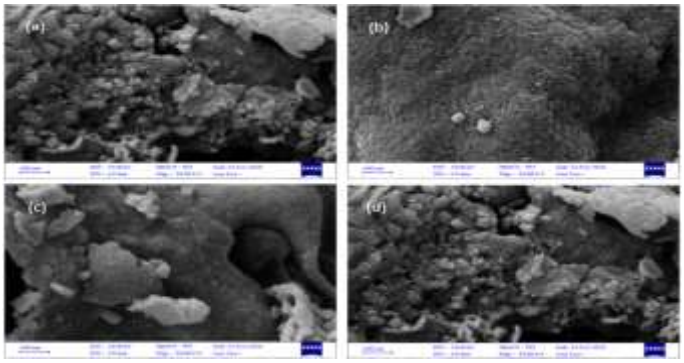

Fig 3: FE-SEM images of $Co_{0.8}Fe_{2.2}O_4$ nanoferrites for (a) as-burnt (b) calcined sample at 500 ℃ (c) at 600 ℃ and (d) at 700 ℃.

The FE-SEM micrographs of the cobalt ferrite powders (Fig.3) demonstrate the predicted microstructure of sol-gel prepared magnetic cobalt ferrite. The as-burnt sample (250 °C) in Fig. 3a revealed a morphology consisting of smaller and agglomerated grains, compared with the image of the other samples. The FE-SEM image revealed that as the calcining temperature raised, the particle size increased. Figure 3 (b-d) displays the FE-SEM image of $Co_{0.8}Fe_{2.2}O_4$ nanoferrites annealed at 500, 600, and 700℃ with some mildly agglomerated and some isolated spherical ferrite particles shown at 700 ˚C due to the thermal process and the naturally happening interaction between magnetic nanoparticles. Table 3 shows that the values of the assessed diameters of the $Co_{0.8}Fe_{2.2}O_4$ nanoparticles for as-burnt and the calcined samples at 500, 600, and 700 ˚C with comparatively well-crystallized grains and mean particle size less than 26.707, 29.964, 39.062, and 53.652 nm, as measured by Image J Software.

Table 3. Average crystallite size and particle size of $Co_{0.8}Fe_{2.2}O_4$ nanoferrites for (a) as-burnt (b) calcined sample at 500 ℃ (c) calcined at 600 ℃ and (d) calcined sample at 700℃ calculated from XRD and FE-SEM

Temp.℃	D(nm) XRD	D(nm) FE-SEM
as-burnt	24.530	26.707
500	27.906	29.964
600	36.265	39.062
700	49.067	53.652

The particle size, which was estimated by FE-SEM micrographs, is found to be larger than that estimated using XRD data. The XRD method could be responsible for the molecular structural disturbance and lattice strain are generated by different ionic radii and/or nanoparticle collection. As a result, it has a more stringent requirement, which results in smaller sizes [21].

The formation of the desired oxide metals is revealed by EDS analysis, suggesting that these metals have undergone chemical reactions. Therefore, the chemical composition of the model and their weight ratios can be determined as illustrated in Figures 4 (a-d). The prominent peaks indicate the major elements in the material (Co, Fe, and O) with the absence of any impurities

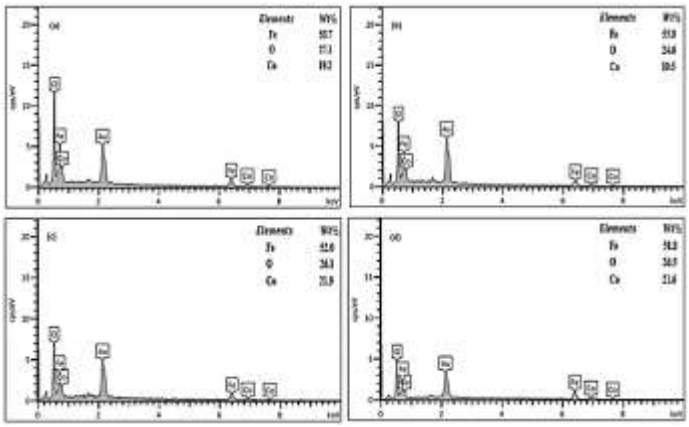

Fig 4: EDS spectra of $Co_{1.2}Fe_{1.8}O_4$ nanoferrites for (a) as-burnt (b) calcined sample at 500℃ (c) at 600 ℃ and (d) at 700 ℃.

3.4. Magnetic Measurement

At room temperature, magnetic hysteresis loops of the $Co_{0.8}Fe_{2.}2O4$ nanoferrites for all synthesized samples were determined using a VSM in an applied field ±15 kOe ranges, as demonstrated in Fig.5.

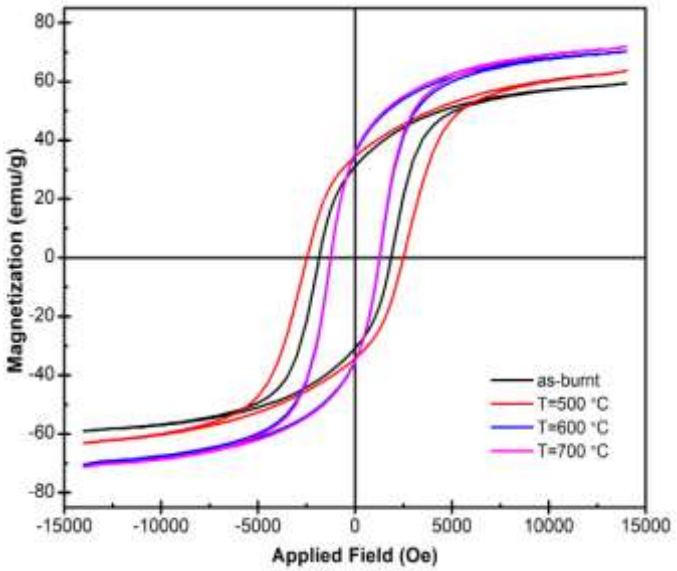

Fig 5**:** Hysteresis curves of $Co_{0.8}Fe_{2.2}O_4$ nanoferrites for as-burnt and different calcination temperatures.

According to the magnetic measurements, all the synthesized ferrite samples show a ferrimagnetic behavior. The magnetic parameters of the cobalt ferrite nanoparticles, such as coercivity (H_c) values, saturation magnetization

values (M_s), and remanent magnetization (M_r) values were obtained from the hysteresis loops. The empirical magnetic moment (n_B), squareness ratio (S), and magnetic anisotropy (K) are determined from the following relationships respectively [21,22].

$$n_B = \frac{(M_{wt} \times M_s)}{5585} \quad (6)$$

$$Remnance\ ratio = \frac{M_r}{M_s} \quad (7)$$

$$H_C = \frac{(0.96 \times K)}{M_s} \quad (8)$$

Where, M_{wt} is the molecular weight.

The shift in saturation magnetization (M_s) in the $Co_{0.8}Fe_{2.2}O_4$ nanoferrites at different calcining temperatures was a major feature observed in the hysteresis loops. The magnetic parameters derived from the hysteresis curves are shown in Table 4. The saturation (M_s) and remanence (M_r) both increase as the calcination temperature rises. The highest saturation magnetization (M_s) was 71.93 emu g^{-1} for the nanoparticles of cobalt ferrite calcined at 700℃ while the smallest saturation magnetization (M_s) was 59.37 emu g^{-1} for as-burnt samples. The shift in saturation magnetization at the calcination temperature increased due to spin canting and surface spin disturbance that occurred in these nanoparticles[16].

Table 4. Variation in saturation magnetization (M_s), remanence magnetization (M_r), coercivity (H_c) magnetic moment (n_B), squareness ratio (M_r / M_s), and magnetic anisotropy (K) of $Co_{0.8}Fe_{2.2}O_4$ nanoferrites for different calcination temperatures.

Temp.℃	M_s (emu g^{-1})	M_r (emu g^{-1})	H_c (O_e)	n_B (μ_B)	M_r/M_s	$K \times 10^3$ (emu .O_e g^{-1})
As-burnt	59.37	31.04	1184.6	2.49	0.52	114.70
500	63.71	34.41	2474.5	2.68	0.54	164.22
600	70.31	35.41	1239.7	2.95	0.50	90.80
700	71.93	36.02	1228.4	3.02	0.50	92.03

Because Fe^{3+} ions have a greater magnetic moment than Co^{2+} ions, the magneton number (η_B) increased from 2.49 to 3.02 μ_B in cobalt ferrite nanoparticles as the calcining temperature increased, resulting in the redistribution of dominant Fe^{3+} ions at B sites. [23]. The coercivity values (H_c) increase from 1854.6 O_e (at as-burnt) to 2474.5 O_e (at 500 ℃) with an increase of calcining temperature . Nonetheless, the coercivity values (H_c) decrease from 2474.5 O_e (at 500 ℃) to 1228.4 O_e (at 700 ℃) with a higher calcining temperature. As a result, the value of coercivity grew until it hit the peak at which point it began to decline. Alternatively, single domain cobalt ferrite nanoparticles create higher coercivity values at lower calcining temperatures, which decrease as calcining progress. This is because the development of multi-domains after the cobalt ferrite nanoparticles exceeds their single-domain size limit [24]. Raghvendra et al. [25] reported that the rise in the effective anisotropy area is related to the increase of coercive values (H_c). According to Néel's two sub-lattice model, the magnetic moments of ferrites are the total of the magnetic moments of individual sub-lattices. In these sub-lattices, ion-electron exchange interaction has various values, ($M = M_B - M_A$) is the overall magnetization, and the A-sublattice magnetization is smaller compared to the B-sublattice magnetization [16]. With an increase in calcining temperature, the anisotropy constant rose from 114.70 × 10^3 emu. $O_e g^{-1}$ (as-burnt) to 164.22 × 10^3 $e$mu . $O_e g^{-1}$ (at 500 ℃). However, with a further increase in the calcining temperature, the anisotropy constant decreased from 164.22 × 10^3 emu. $O_e g^{-1}$ (at 500 ℃) to 90.80 × 10^3 emu. $O_e g^{-1}$ (at 600 ℃). As a result, due to a decrease in average crystalline size, cationic redistribution changed in the magnetic domain regime, affecting magnetocrystalline anisotropy [24]. The squareness ratio of (M_r/M_s) sheds light on the investigated ferrite nanoparticles' superexchange interactions and magnetocrystalline anisotropy [8]. Our findings elucidate that the values of (M_r/M_s) are approximately larger than 0.5. As a result, the nanoparticles' have superexchange interactions [16].

3.5. Dielectric Properties

The dielectric properties of ferrite nanoparticles provide insight into the electrical conduction process in terms of dielectric reaction in an *AC* electric field. A multitude of factors influences these qualities, including chemical composition, the method of preparation, stoichiometry, ionic charge, grain size, porosity, and cation distribution between the tetrahedral and octahedral structures [14].

Dielectric properties of the synthesized materials such as the real part of the dielectric constant($\acute{\varepsilon}$), the imaginary part of the dielectric loss (ε") or dielectric loss factor, dielectric loss angle ($tan\ \delta$), and AC conductivity (σ_{ac}) are calculated as a function of frequency (200 kHz – 2 MHz) for different temperatures of $Co_{0.8}Fe_{2.2}O_4$ as shown in table 5. using the following relationships [26].

$$\acute{\varepsilon} = \frac{Cd}{\varepsilon_o\ A} \quad (9)$$

$$\tan\delta = \frac{1}{2\pi f R_p C_p} \quad (10)$$

$$\varepsilon^{''} = \acute{\varepsilon} \tan\delta \quad (11)$$

$$\sigma_{ac} = 2\pi f \varepsilon_o\ \acute{\varepsilon} \tan\delta \quad (12)$$

Where C is the capacitance of the pellet in farad, d is the thickness of the pellet in meter, A the cross-sectional area of the flat surface of the pellet, ε_o is the constant of permittivity of free space, R_p is the equivalent parallel resistance, C_p is the equivalent parallel capacitance, and f is the frequency.

The dielectric constant(ε'), dielectric loss angle ($tan\ \delta$), dielectric loss factor (ε''), and *AC* conductivity (σ_{ac}) as a function of frequency, are represented in Fig. 6(a-d). The

dielectric constant (ε') declines as the frequency increases until it reaches its minimum value in a higher frequency region, indicating frequency dispersion in the low-frequency range. This was observed in the majority of ferrite materials. [27]. The presence of many types of polarization (electronic, dipolar, ionic, etc.) including space charge, which dominates at low frequency, could explain the high values of dielectric constant (ε') at low frequency [14]. According to Koop's theory, the Maxwell-Wagner form of dispersion is represented by a reduction in dielectric constant (ε') as frequency increases [28]. In $Co_{0.8}Fe_{2.2}O_4$, local electron displacement in the direction of the applied field is caused by electron exchange between the two iron ions (Fe^{2+} and Fe^{3+}) at the octahedral site[17].

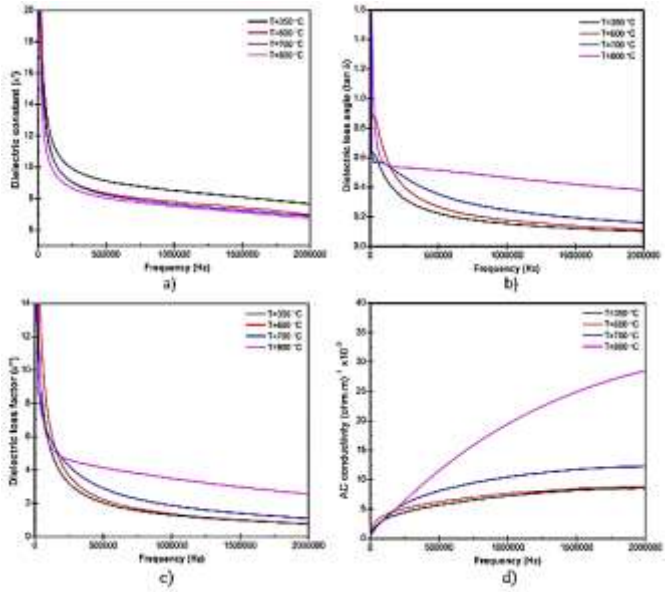

Fig 6: Dielectric properties of $Co_{0.8}Fe_{2.2}O_4$ nanoferrites as a function of frequency, (a) dielectric constant(ε'), (b) dielectric loss angle (tan δ), (c) dielectric loss factor (ε''), and (d) AC conductivity (σ_{ac}).

The polarization can be described by electron hopping between ferrous ions (Fe^{2+}) and ferric ions (Fe^{3+}) ions and hole hopping between Co^{2+} and Co^{3+} in the octahedral sites, according to the Rezlescue Model [8]. The frequency of electron/hole interaction will be unable to follow the applied electric field in the higher frequency region, resulting in polarization loss. As a result, the dielectric permittivity approaches a constant value at higher frequencies. The conductivity of a polycrystalline material has been shown to increase with increasing particle size. Smaller grains imply a smaller grain-to-grain surface contact area, and thus less electron movement [8].

The variance of dielectric loss factor (ε'') with frequency as displayed in Figure (c), indicates a decrease with the increase in the frequency. However, in the higher frequency range, the rate of loss slowed and essentially leveled off, which is consistent with Koop's thesis. Interfacial regions, such as the material's surface, have grain boundaries that are poorly conducted, active, and require higher energy for electron hopping. In the high-frequency zone, the highly conducting grains get active, decreasing the energy required for hopping [29].

The AC conductivity (σ_{ac}) variation regarding the applied frequency of $Co_{0.8}Fe_{2.2}O_4$ nanoparticle, at various sintering temperatures, is depicted in Fig.6(d). The AC conductivity progressively rises as the frequency of the applied field increases and it rises steadily at higher frequencies. At lower frequencies, grain boundaries are more active, resulting in minimal electron hopping between Fe^{2+} and Fe^{3+} ions, which in turn leads to low conductivity and bound at lower frequencies. It is evident from the figure that the frequency dependence of AC conductivity grows. However, as the frequency increases, the conductivity increases progressively due to electron hopping between Fe^{2+} and Fe^{3+} ions on the B sites [10].

The frequency-dependent variance of AC electrical conductivity has been established using Maxwell – Wagner's dielectric double layer model. As a result, grain boundaries perform better at lower frequencies. At lower frequencies, the electron hopping frequency between Fe^{2+} and Fe^{3+} is considerably reduced. As a result, the materials' apparent conductivity at lower frequencies is decreased. The conductive grains, on the other hand, become more effective as the frequency of the applied field increases, encouraging electron hopping between adjacent ions by promoting hopping between Fe^{2+} and Fe^{3+} ions on the octahedral sites. As a result, as the frequency rises, the electrical conductivity increases as well [14].

Figure 6 (a) indicates the variation of the dielectric constant of $Co_{0.8}Fe_{2.2}O_4$ nanoparticles as a function of frequency. A decrease in dielectric constant appears at 200KHz, 500KHz, 1MHz, 1.5MHz, and 2MHz degrees with the increase in the temperatures 600, 700, and 800℃. The nature of the variation in the dielectric constant is consistent with previous results for manganese doped cobalt ferrite nanoparticles as reported in the literature [30]. The decreasing pattern in dielectric constant at temperatures 600, 700, and 800 ℃ may be attributed to the conversion of interfacial polarization to ionic polarization because of charge hopping between Co^{2+} and Fe^{2+} ions in the B site [31].

The variation of the dielectric loss angle of $Co_{0.8}Fe_{2.2}O_4$ nanoparticles as a frequency function is shown in Figure 6 (b). The dielectric loss angle increases as the temperature rise at 200 kHz, 500KHz, 1MHz, 1.5MHz, and 2MHz degrees. The increase in dielectric loss angle (tan δ) caused by electrical conductivity is greater than that caused by relaxation effects[32]. Figure 6 (c) indicates the variation of the dielectric loss factor of $Co_{0.8}Fe_{2.2}O_4$ nanoparticles as a function of frequency. An increase in dielectric loss factor

appears at 200KHz, 500KHz, 1MHz, 1.5MHz, and 2MHz degrees with the increase in the temperatures 600, 700, and 800℃. Similar results were reported for gadolinium substituted nickel ferrite [29]. A rise in conductivity appears at temperatures 600, 700, and 800℃. The increase in AC conductivity at higher temperatures can be ascribed to the thermally stimulated greater flexibility of charge carriers which results in further electron transfer from one ion to another [33].

Table 5. Values of dielectric constant (ε'), dielectric loss angle ($tan\ \delta$), dielectric loss factor (ε'') and AC conductivity (σ_{ac}) at 200 KHz, 500 KHz, 1 MHz, 1.5 MHz and 2 MHz for $Co_{0.8}Fe_{2.2}O_4$ sintered at 350℃ 600℃, 700℃, and 800℃.

$Co_{0.8}Fe_{2.2}O_4$	350℃	600℃	700℃	800℃
ε' (200KHz)	10.3	9.39	9.38	8.92
tan δ (200KHz)	0.360	0.458	0.500	0.536
ε" (200KHz)	3.75	4.35	4.74	4.83
σ_{ac} (200KHz)×10^{-5}	4.12	4.78	5.22	5.33
ε' (500KHz)	9.12	8.34	8.23	8.03
tan δ (500KHz)	0.224	0.268	0.354	0.516
ε" (500KHz)	2.09	2.29	2.96	4.19
σ_{ac} (500KHz)×10^{-5}	5.69	6.22	8.11	11.5
ε' (1MHz)	8.51	7.78	7.64	7.50
tan δ (1MHz)	0.153	0.177	0.246	0.466
ε" (1MHz)	1.35	1.43	1.92	3.55
σ_{ac} (1MHz) ×10^{-5}	7.26	7.66	10.4	19.5
ε' (1.5MHz)	8.08	7.30	7.24	7.12
tan δ (1.5MHz)	0.122	0.139	0.194	0.420
ε" (1.5MHz)	0.98	1.01	1.45	3.03
σ_{ac} (1.5MHz) ×10^{-5}	8.22	8.44	11.7	24.9
ε' (2MHz)	7.63	6.97	6.87	6.74
tan δ (2MHz)	0.101	0.113	0.161	0.382
ε" (2MHz)	0.77	0.79	1.15	2.62
σ_{ac} (2MHz) ×10^{-5}	8.42	8.75	12.2	28.5

4. CONCLUSIONS

The sol-gel auto combustion method was used to prepare $Co_{0.8}Fe_{2.2}O_4$ nanoferrites. Various characterization techniques such as FT-IR, XRD, FE-SEM EDS, and VSM, were used to examine the effect of calcination temperature on crystallinity, phase structure, morphology, and magnetic properties. X-ray diffraction and FT-IR measurements revealed that all samples displayed the typical behavior of a nanoparticle with a single-phase spinel shape. Thermal treatments were observed to affect the hopping length, crystallite size, x-ray density, and lattice parameter. EDS was used to characterize the composition and verify the existence of O, Co, Fe, in all samples. The particle size increases as the calcination increases, as shown by FE-SEM photographs. Magnetization measurement indicated that the highest value of coercivity (H_c), saturation magnetization (M_s) and remanence magnetization (M_r) were obtained at calcining temperatures 500 and 700 ℃, respectively. The dielectric constant (ε') and dielectric loss factor (ε'') and the dielectric loss angle ($tan\delta$) decreased as frequency rose, then became constant at high frequencies, perhaps due to electron hopping between ferrous (Fe^{2+}) and ferric (Fe^{3+}) ions. The levels of dielectric loss are minimal at higher frequencies, indicating that high-frequency applications may be conceivable. In all samples, the dielectric constant and AC conductivity follow Koop's theory, the Maxwell-Wagner polarization process, and electron hopping, with conductivity (σ_{ac}) increasing with frequency.

5. REFERENCES

[1] A. Goldman, *Modern ferrite technology*: Springer Science & Business Media, 2006.

[2] S. W. Lee, S. Bae, Y. Takemura, I.-B. Shim, T. M. Kim, J. Kim, H. J. Lee, S. Zurn, C. S. Kim, "Self- heating characteristics of cobalt ferrite nanoparticles for hyperthermia application," *Journal of Magnetism and Magnetic Materials*, vol. 310, no. 2, pp. 2868-2870, 2007.

[3] U. Häfeli, W. Schütt, J. Teller, and M. Zborowski, *Scientific and clinical applications of magnetic carriers*: Springer Science & Business Media, 2013.

[4] S. Singh, S. Munjal, and N. Khare, "Strain/defect induced enhanced coercivity in single domain $CoFe_2O_4$ nanoparticles," *Journal of Magnetism and Magnetic Materials*, vol. 386, pp. 69-73, 2015.

[5] M. P. Reddy, A. Mohamed, X. Zhou, S. Du, and Q. Huang, "A facile hydrothermal synthesis, characterization and magnetic properties of mesoporous $CoFe_2O_4$ nanospheres," *Journal of Magnetism and Magnetic Materials*, vol. 388, pp. 40-44, 2015.

[6] R. Mohamed, M. Rashad, F. Haraz, and W. Sigmund, "Structure and magnetic properties of nanocrystalline cobalt ferrite powders synthesized using organic acid precursor method," *Journal of Magnetic Materials*, vol. 322, no. 14, pp. 2058-2064, 2010.

[7] V. Cabuil, V. Dupuis, D. Talbot, and S. Neveu, "Ionic magnetic fluid based on cobalt ferrite nanoparticles: influence of hydrothermal treatment on the nanoparticle size," *Journal of Magnetism and Magnetic Materials*, vol. 323, no. 10, pp. 1238-1241, 2011.

[8] E. V. Gopalan, P. Joy, I. Al-Omari, D. S. Kumar, Y. Yoshida, and M. Anantharaman, "On the structural, magnetic and electrical properties of sol-gel derived nanosized cobalt ferrite," *Journal of Alloys and Compounds*, vol. 485, no. 1-2, pp. 711-717, 2009.

[9] M. B. Mohamed, and M. Yehia, "Cation distribution and magnetic properties of nanocrystalline gallium substituted cobalt ferrite," *Journal of Alloys and Compounds*, vol. 615, pp. 181-187, 2014.

[10] S. I. Ahmad, A. Rauf, T. Mohammed, A. Bahafi, D. R. Kumar, and M. B. Suresh, "Dielectric, impedance, AC conductivity and low-temperature magnetic studies of Ce and Sm co-substituted nanocrystalline cobalt ferrite,"

Journal of Magnetism and Magnetic Materials, vol. 492, pp. 165666,2019.

[11] P. Roy, and J. Bera, "Enhancement of the magnetic properties of Ni–Cu–Zn ferrites with thesubstitution of a small fraction of lanthanum for iron," *Materials research bulletin*, vol. 42, no. 1, pp.77- 83, 2007.

[12] M. Goodarz Naseri, E. B. Saion, H. Abbastabar Ahangar, A. H. Shaari, and M. Hashim, "Simple synthesis and characterization of cobalt ferrite nanoparticles by a thermal treatment method," *Journalof Nanomaterials*, vol. 2010, 2010.

[13] A. Mohammad, S. ALIRIDHA, and T. Mubarak, "STRUCTURAL AND MAGNETIC PROPERTIES OF Mg-Co FERRITE NANOPARTICLES," *Digest Journal of Nanomaterials & Biostructures (DJNB)*, vol. 13, no. 3, 2018.

[14] A. M. Mohammad, S. M. A. Ridha, and T. H. Mubarak, "Dielectric properties of Cr-substituted cobalt ferrite nanoparticles synthesis by citrate-gel auto combustion method," *Int. J. Appl. Eng. Res*, vol. 13, no. 8, pp. 6026-6035, 2018.

[15] Z. Rouhani, J. Karimi-Sabet, M. Mehdipourghazi, A. Hadi, and A. Dastbaz, "Response surfaceoptimization of hydrothermal synthesis of Bismuth ferrite nanoparticles under supercritical water conditions: Application for photocatalytic degradation of Tetracycline," *Environmental Nanotechnology, Monitoring & Management*, vol. 11, pp. 100198, 2019.

[16] A. Mohammad, M. Mohammed, and L. Hussein, "STRUCTURAL, MAGNETIC AND OPTICAL PROPERTIES OF $Co_{0.5}Ni_{0.5}Fe_2O_4$ NANOPARTICLES SYNTHESIZED BY SOL-GEL AUTO COMBUSTION METHOD," *DIGEST JOURNAL OF NANOMATERIALS AND BIOSTRUCTURES*,vol. 15, no. 1, pp. 231-241, 2020.

[17] R. Zhang, L. Sun, Z. Wang, W. Hao, E. Cao, and Y. Zhang, "Dielectric and magnetic properties of $CoFe_2O_4$ prepared by sol-gel auto-combustion method," *Materials Research Bulletin*, vol. 98, pp. 133-138, 2018.

[18] M. Kurian, S. Thankachan, D. S. Nair, E. Aswathy, A. Babu, A. Thomas, and B. K. KT, "Structural, magnetic, and acidic properties of cobalt ferrite nanoparticles synthesised by wet chemical methods," *Journal of Advanced Ceramics*, vol. 4, no. 3, pp. 199-205, 2015.

[19] R. S. Yadav, J. Havlica, J. Masilko, L. Kalina, J. Wasserbauer, M. Hajdúchová, V. Enev, I. Kuřitka, and Z. Kožáková, "Impact of Nd^{3+} in $CoFe_2O_4$ spinel ferrite nanoparticles on cation distribution, structural and magnetic properties," *Journal of Magnetism and Magnetic materials*, vol. 399, pp. 109-117, 2016.

[20] M. Eltabey, A. Massoud, and C. Radu, "Microstructure and superparamagnetic properties of Mg-Ni-Cd ferrites nanoparticles," *Journal of Nanomaterials*, vol. 2014, 2014.

[21] C. Ragupathi, J. J. Vijaya, L. J. Kennedy, and M. Bououdina, "Combustion synthesis, structure, magnetic and optical properties of cobalt aluminate spinel nanocrystals," *Ceramics International*, vol. 40, no. 8, pp. 13067-13074, 2014.

[22] T. Prabhakaran, and J. Hemalatha, "Chemical control on the size and properties of nano $NiFe_2O_4$synthesized by sol–gel autocombustion method," *Ceramics International*, vol. 40, no. 2, pp. 3315-3324, 2014.

[23] B. Purnama, and A. T. Wijayanta, "Effect of calcination temperature on structural and magneticproperties in cobalt ferrite nano particles," *Journal of King Saud University-Science*, vol. 31, no. 4,pp. 956-960, 2019.

[24] R. S. Yadav, J. Havlica, J. Masilko, L. Kalina, M. Hajdúchová, V. Enev, J. Wasserbauer, I. Kuřitka, and Z. Kozakova, "Structural, Cation Distribution, and Magnetic Properties of $CoFe_2O_4$ Spinel Ferrite Nanoparticles Synthesized Using a Starch-Assisted Sol–Gel Auto-Combustion Method," *Journal ofSuperconductivity and Novel Magnetism*, vol. 28, no. 6, pp. 1851-1861, 2015.

[25] R. S. Yadav, J. Havlica, M. Hnatko, P. Šajgalík, C. Alexander, M. Palou, E. Bartoníčková, M. Boháč,F. Frajkorová, and J. Masilko, "Magnetic properties of $Co_{1-x}Zn_xFe_2O_4$ spinel ferrite nanoparticlessynthesized by starch-assisted sol–gel autocombustion method and its ball milling," *Journal ofMagnetism and Magnetic Materials*, vol. 378, pp. 190-199, 2015.

[26] M. Raghasudha, D. Ravinder, and P. Veerasomaiah, "Influence of Cr^{3+} ion on the dielectric properties of nano crystalline Mg-ferrites synthesized by citrate-gel method," 2013.

[27] K. M. Batoo, and M.-S. Abd El-sadek, "Electrical and magnetic transport properties of Ni–Cu–Mg ferrite nanoparticles prepared by sol–gel method," *Journal of alloys and compounds*, vol. 566, pp. 112-119, 2013.

[28] M. Cernea, P. Galizia, I. Ciuchi, G. Aldica, V. Mihalache, L. Diamandescu, and C. Galassi, "$CoFe_2O_4$ magnetic ceramic derived from gel and densified by spark plasma sintering," *Journal of Alloys and Compounds*, vol. 656, pp. 854-862, 2016.

[29] M. M. L. Sonia, S. Anand, V. M. Vinosel, M. A. Janifer, S. Pauline, and A. Manikandan, "Effect of lattice strain on structure, morphology and magneto-dielectric properties of spinel $NiGd_xFe_{2-x}O_4$ ferrite nano-crystallites synthesized by sol-gel route," *Journal of Magnetism and Magnetic Materials*, vol. 466, pp. 238-251, 2018.

[30] M. Ahsan, and F. Khan, "Structural and electrical properties of manganese doped cobalt ferritenanoparticles," *Mater Sci. Nanotechnol.(2018) 2 (2): 1*, vol. 9, 2018.

[31] R. Nongjai, S. Khan, K. Asokan, H. Ahmed, and I. Khan, "Magnetic and electrical properties of In doped cobalt ferrite nanoparticles," *Journal of Applied Physics*, vol. 112, no. 8, pp. 084321, 2012.

[32] R. Rani, G. Kumar, K. M. Batoo, and M. Singh, "Influence of temperature on the electric, dielectricand AC conductivity properties of nano-crystalline zinc substituted cobalt ferrite synthesized by solution combustion technique," *Applied Physics A*, vol. 115, no. 4, pp. 1401-1407, 2014.

[33] S. Suresh, "Synthesis, structural and dielectric properties of zinc sulfide nanoparticles," *International Journal of Physical Sciences*, vol. 8, no. 21, pp. 1121-1127, 2013.

P- ISSN 1991-8941 E-ISSN 2706-6703 *Journal of University of Anbar for Pure Science (JUAPS)* Open Access
2021,15 (2) :74 –82

تحضير وتشخيص جسيمات فيرايت السبنل $Co_{0.8}Fe_{2.2}O_4$ النانوية

محمد برهان جمعه[1] و تحسين حسين مبارك[1] و علي مصطفى محمد[2]
[1]جامعة ديالى ، كلية العلوم ، قسم الفيزياء
[2]جامعة كرميان ، كلية التربية ، قسم الفيزياء
sciphyms06@uodiyala.edu.iq

الخلاصة:

حضرت جسيمات فيرايت الكوبلت $Co_{0.8}Fe_{2.2}O_4$ النانوية باستخدام تقنية الاحتراق التلقائي للهلام. تمت دراسة تأثير درجة حرارة الكلسنة على الخصائص التركيبية والمغناطيسية والكهربائية. تم تأكيد تشكيل الطور السبنل المكعبي لتركيب الفيرايت باستخدام مطيافية الأشعة تحت الحمراء (FT-IR) وأنماط حيود الأشعة السينية (XRD). اذ تراوحت حجم البلورات المتكونة لعينات الفيرايت من 24.530 إلى 49.067 نانومتر ووجد أنها تعتمد على درجة حرارة الكلسنة. وفقًا لصور المجهر الإلكتروني الماسح ذي الانبعاث المجالي (FE-SEM) يزداد حجم الجسيمات مع ارتفاع درجة حرارة الكلسنة. تم استخدام طيف تشتت الطاقة (EDS) لتأكيد وجود Co و Fe و O في جميع العينات. تم استخدام جهاز (VSM) لدراسة الخصائص المغناطيسية للعينات المحترقة والمكلنسة مثل القوة القهرية (H_c) ، التشبعية المغناطيسية (M_s) ، التخلفية المغناطيسية (M_r) . أظهرت جميع العينات سلوكاً فيري مغناطيسياً ، تبين انه مع ارتفاع درجة حرارة الكلسنة ، تزداد التشبعية المغناطيسية ، التخلفية المغناطيسية والنسبة بين قيم (M_r/M_s). يرتبط هذا السلوك بانتعاش الدوران والاضطراب في دوران السطح عند درجة حرارة الغرفة. تم فحص عامل الفقد العزلي (ε'') وظل الفقد العزلي $(\tan\delta)$ وثابت العزل الكهربائي (ε') و وتوصيلية الكهربائية (σ_{ac}) لجميع العينات كدالة للتردد باستخدام مقياس LCR. تم دراسة التغييرات في خصائص العزل الكهربائي في مدى تردد (50Hz-2MHz) استنادًا إلى نظرية كوبس واستقطاب ماكسويل - فاجنر والتنقل الإلكتروني مع زيادة التردد ، أظهرت الخصائص العزل الكهربائي بالكامل سلوكًا طبيعيًا.